Springer

KSME

Journal of Mechanical Science and Technology 30 (2) (2016) 925~932
www.springerlink.com/content/1738-494x(Print)/1976-3824(Online)
DOI 10.1007/s12206-016-0146-1

# Experimental investigations on combustion characteristics of a swirl-stabilized premixed burner †

Ju Hyeong Cho[1,*], Han Seok Kim[1], Min Kuk Kim[1], Jeong Jae Hwang[1], Sang Min Lee[1] and Ta Kwan Woo[2]

[1]*Korea Institute of Machinery and Materials, Daejeon, 305-343, Korea*
[2]*SUNG-IL Turbine Co., Busan, 618-818, Korea*

(Manuscript Received May 2, 2015; Revised September 14, 2015; Accepted October 5, 2015)

**Abstract**

Experimental investigations have been conducted to understand the combustion characteristics of a swirl-stabilized double-cone premixed burner used for industrial gas turbines for power generation. NOx and CO emissions, extinction limit, combustion noise, pressure loss, and wall temperature distributions were measured for various operating conditions. Results show that NOx emissions are decreased with increasing air/fuel ratio or decreasing air load unless the air load is too small. CO emissions are also decreased with increasing air/fuel ratio, leading to a positive correlation between NOx and CO emissions. Flame extinction limit is reduced with increasing air flow rate as the flow residence time is reduced. Combustion noise has its peak amplitude at the frequencies of 150 or 300 Hz, which are considered to be the resonance frequencies of the longitudinal mode of the combustor. The noise level at the peak frequency is maximized when the flame is considered to be located near the burner exit. Pressure loss is decreased with the A/F ratio as the flame moves downstream out of the burner.

*Keywords*: Gas turbine; Swirl-stabilized premixed burner; Combustion; Emissions; Pressure loss

## 1. Introduction

As environmental regulations have continued to become more stringent in the context of NOx emissions in industrial applications, including stationary gas turbines and power generation systems, the concept of lean premixed combustion has gained increasing attention as a promising means of meeting the requirement of emission goals while maintaining the system operability [1].

Though the design philosophies and implementation methods of lean premixed burners are varying among major gas turbine manufacturers, the key features of achieving low pollutant emissions are based on premixing fuel and air in lean conditions to reduce adiabatic flame temperature, leading to less production of thermal NOx. The degree of premixing is also important because making the mixture of fuel and air as uniform as possible enables reduction of hot spots, leading also to reduction of thermal NOx production. Premixing is usually enhanced by use of radial or axial types of swirlers in the passage of air flow, as demonstrated, for instance, by GE [2], Alstom [3], Siemens [4], Pratt and Whitney [5] and Solar Turbines [6].

Among these, Alstom's EV burner (environmental friendly V-shaped burner) is featured by the flame stabilizing mechanism driven from fundamental principles of vortical flows. It utilizes the vortex breakdown of a strongly swirling core flow, which serves as an aerodynamic control for the inner recirculation zone to stabilize a premix flame, without the need for a swirler body or specific flame stabilizer.

The EV burner consists of two half-cone shells that are offset perpendicular to the axis, generating two tangential slots, as shown in Fig. 1. Air flow entering through the tangential slots is mixed with fuel injected from the manifold along the tangential slots. The swirl strength of the mixture is increased in axial direction as the mixture rotates along the inner surface of the cone, and a vortex breakdown of the core flow occurs close to the burner exit.

What is currently known as the EV burner is the second generation of this type of burner. Designed to have short but effective premixing zones, it has overcome the main drawbacks that the first generation had: too long a premix tube that paused with viable chance of autoignition or flashback. The EV burner, designated as the second generation of the EV burner hereafter, was first implemented in the single silo-type combustor of a GT11, where 36 burners plus a central ignition

*Corresponding author. Tel.: +82 42 868 7083, Fax.: +82 42 868 7284
E-mail address: antocho@kimm.re.kr
† Recommended by Associate Editor Jeong Park

burner were arranged in a hexagonal arrangement. It has been further implemented in their models of GT13, GT24/26, for example, achieving NOx levels well below 25 vppmd (@15%$O_2$) [3, 7].

Various attempts for investigations associated with combustion characteristics of the EV burner in terms of emissions and stabilities have been reported in a number of publications, for example, Paschereit et al. [8], Zajadatz et al. [9], Kokanović et al. [10], Fritsche et al. [11], etc., some of which use a scaled-down burner.

The present study is to understand the characteristics of a conical EV burner in terms of combustion and aerodynamic characteristics such as emissions, stability, combustion noise, and pressure loss. Surface temperature distributions are also measured to indirectly anticipate the flame location and also provide temperature data referenced for TBC (Thermal barrier coating). A single burner in full scale was experimentally investigated instead of using a downscaled one to demonstrate the characteristics of an actual burner which is applied to the GT11N gas turbine with a base load of 80 MWe, manufactured by the former ABB (later ALSTOM Power).

## 2. Experimental setup

### *2.1 Test rig design and system configuration*

Fig. 1 shows the overall configuration of the atmospheric combustion test system. NG (Natural gas) is used as a fuel. Air is supplied by two turbo-compressors with maximum air flow rate of 1.4 kg/s at 6 bar in absolute pressure. Flow rates of fuel and air are measured by the Coriolis flowmeter (Micro-motion). The exhaust gas is sampled through a water-cooled sampling probe and fed into the gas analyzer (MK2 Greenline) for measurement of NOx, CO, $O_2$ emissions. Flame image is recorded using a camcorder (SONY HDR-CX130). Combustion noise is measured by a microphone (MPA215) located just outside the windbox pointing the burner. Frequency characteristics of combustion noise are analyzed with an in-house FFT code with a sampling rate of 44100 Hz. The pressure drop across the burner is measured with a digital pressure transmitter. Temperature is measured at the front exit and the conical part of the burner and along the surface of the combustion liner using K-type thermocouples.

The combustion chamber, in which the conical burner is installed, consists of an outer casing, a windbox, and a combustion liner. The outer casing surrounds the combustion liner such that the pre-heated air passes through the annulus between the casing and the liner in a direction opposite to the flow direction of the combustion gas inside the liner. As such, additional heat transfer from the hot combustion gas to the supplied air enables the air temperature to reach the required temperature of 370°C at the burner inlet. The supplied air in the silo-type combustor of GT11N is considered to be quite uniform as the supplied air passes through a relatively large space before it enters a bundle of 36 EV burners. In this study, as the windbox can accommodate only a single burner with a limited space, securing uniformity of the supplied air through the windbox was one of the major concerns in designing the combustion chamber. To enhance the uniformity of the supplied air, an annular plate with several holes is placed upstream of the windbox as shown in Fig. 1(b). Numerical simulation using commercial software CFD-ACE was utilized to determine the number and size of the holes on the annular plate which gives the best uniformity in the flow velocity through the holes with moderate flow patterns in the windbox.

Table 1. Experimental test conditions.

| Parameter | Unit | Value | Remarks |
|---|---|---|---|
| Air flow rate | kg/s | 0.5 | Air Load 1.0 |
| Fuel flow rate | kg/hr | 49.95 | Design point |
| A/F (Air-to-fuel ratio) | kg/kg | 36.0 | Design A/F |
| Inlet air temperature | °C | 370 | |

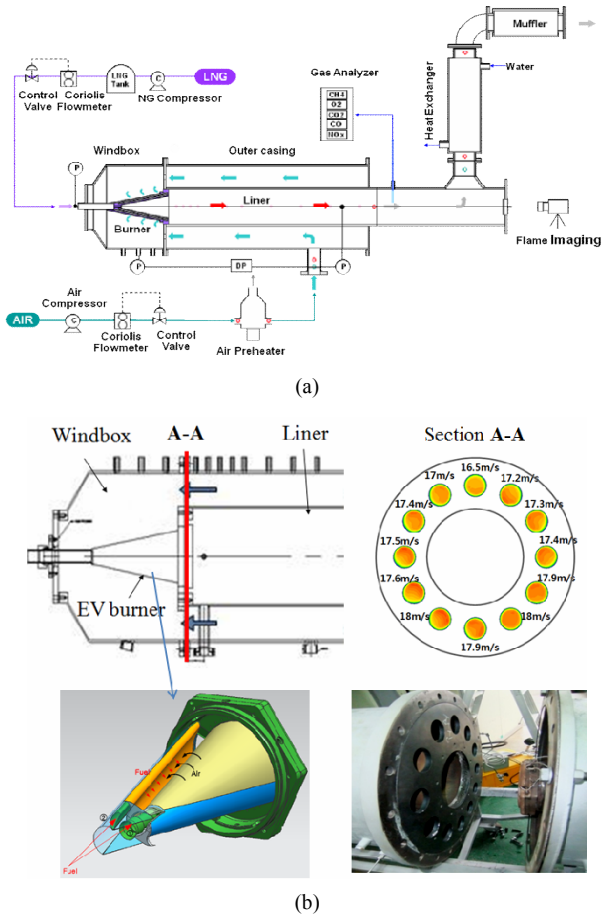


Fig. 1. Schematic of combustion test system: (a) System configuration; (b) windbox with an EV burner.

### *2.2 Test conditions*

Experimental tests were conducted at ambient pressure for a single full-scaled burner. The ambient test conditions for fuel

and air flow rates were evaluated from the operation data of GT11N power plant. The resultant test conditions are shown in Table 1.

## 3. Results and discussion

### *3.1 NOx and CO emissions*

Fig. 2 shows the dependence of NOx emissions on the exhaust $O_2$ emissions for various air loads. Air load is defined in this study as the air flow rate normalized by the reference air flow rate of 0.5 kg/s. Since the aerodynamic condition such as air flow velocity at the burner exit is kept invariant for each air load, the fuel flow rate is then adjusted with each air load in the range of the A/F ratio from 31.7 up to a blowoff condition to decouple the effect of burning velocity from that of flow velocity. NOx emissions, which are normalized by the maximum value of NOx emissions for the air load of 1, are decreased overall with an increase in the exhaust $O_2$ emissions, i.e., an increase in the A/F ratio, because a higher A/F ratio results in a lower adiabatic flame temperature, leading to reduction of thermal NOx. The dependence of NOx emissions on air load seems to be more complicated as observed in Fig. 2. This is partly due to the trade-off between heat loss and residence time that acts in an opposite way in the context of NOx emissions, and partly due to the flame location and the degree of premixing of fuel and air. As the air load is reduced from 1.0 to 0.8, the relative heat loss over the heat liberated from the combustion is increased due to a reduced flame size; i.e. a ratio of the heat loss (~$D^2$ with an overall flame size of D) to the heat liberation (~$D^3$) yields a 1/D dependence, resulting in reduction of the flame temperature which leads to reduction of the thermal NOx. In this case, it seems that the NOx increase due to a longer residence time does not play as significant a role as NOx reduction due to an increase in the relative heat loss. When the air load is further reduced from 0.8 to 0.6, NOx is further decreased due to an increased heat loss for a lower A/F ratio corresponding to the exhaust $O_2$ of less than 11%. However, for a higher A/F ratio corresponding to the exhaust $O_2$ of greater than 11%, the rate of NOx reduction with exhaust $O_2$ is not as large as it is for higher air loads. It is considered that, for an air load of 0.6, the flame moves further upstream toward the interior of the cone and a significant part of flame stays inside the cone, which implies that the quality of fuel-air mixing is degraded due to a shorter mixing distance to the flame, resulting in more hot spots in the flame, which leads to an increase in thermal NOx emissions. The smallest air flow rate for the air load of 0.6 also attenuates the recirculation strength of the product gases in reaction zones, which diminishes the beneficial effect of the vitiated product gases on NOx reduction. Which effect would be more dominant among the fore-mentioned effects on NOx emissions is considered to depend on the operating conditions as well as the geometry of burners that determine aerodynamic and mixing characteristics.

Fig. 3 shows the dependence of CO emissions on the exhaust $O_2$ emissions for various air loads for the same conditions shown in Fig. 2. CO emissions, which are normalized by the maximum value of CO emissions for the air load of 1, are decreased with an increase in the exhaust $O_2$ emissions because a larger amount of excess air facilitates the oxidation of CO into $CO_2$. Fig. 4 shows the relation between NOx and CO emissions, the data of which are extracted from Figs. 2 and 3. The overall trend of NOx vs. CO demonstrates that CO increases with an increase in NOx for a given heat load, which

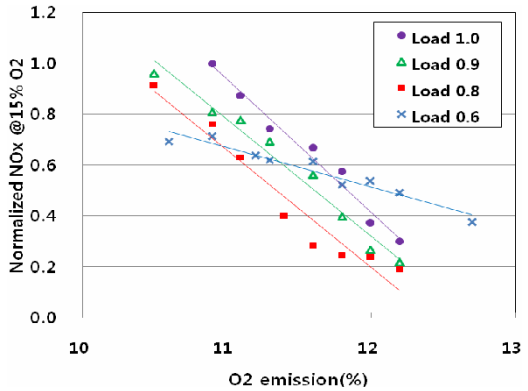


Fig. 2. The dependence of NOx emissions on the exhaust $O_2$ emissions for various air loads.

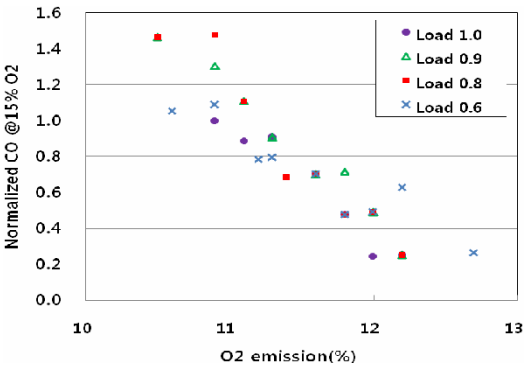


Fig. 3. The dependence of CO emissions on the exhaust $O_2$ emissions for various air loads.

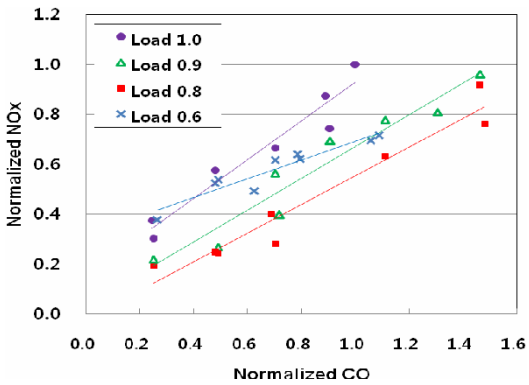


Fig. 4. The relation between NOx and CO emissions for various air loads.

coincides with Sattelmayer et al. [12] Such trend of CO increase with NOx increase implies that, when the A/F ratio is decreased, the kinetic limitation due to less amount of available oxidizer, i.e., a reduced oxidation of CO into $CO_2$, plays a more significant role than CO dissociation due to an increased adiabatic flame temperature.

### *3.2 Flame images and temperature distributions*

Fig. 5 shows the flame images observed from the downstream side of the burner for various A/F ratios. The blue color inside the circular liner represents the flame. The flame luminosity inside the hexagonal shape of the burner is brightest at the lowest A/F ratio of 34.4 as the flame temperature is highest. Then the luminosity at the center of the burner fades away and spreads outwards in a radial direction with an increase in A/F ratio. This implies that the flame is initially located inside the burner at lower A/F ratios because of a higher burning rate, while the flame moves out of the burner as the A/F ratio is increased.

Fig. 6 shows temperature distributions on the burner tip face for various A/F ratios and air loads. Temperature was measured using K-type thermocouples at three corners of the hexagonal face of the burner tip. The tip temperatures range from about 650 to 850°C. For the air load of 1, as shown in Fig. 6(a), the temperature of CH25 is highest and that of CH26 is lowest, which means that the reaction rate is not uniform in a circumferential direction at the burner exit, i.e., the flame is closest to the CH25 and the air supplied through the air slot seems to directly reach the middle point, CH26. The tip temperatures are slightly increased and then decreased with their peaks at an A/F ratio of around 36. This implies that when the A/F ratio is lower than 36, a larger part of the flame sits inside the cone, allowing less portion of the flame to view the cone tip face, leading to the decrease in the temperature on the tip face. On the other hand, when the A/F ratio is higher than 36, the flame shifts from the interior of the cone toward the outside of the cone due to a reduced flame speed, moving away from the cone tip face, leading also to the decrease in the temperature on the tip face. For a smaller air load of 0.8, as shown in Fig. 6(b), the peak temperatures are reduced by about 50 degrees in comparison with Fig. 6(a). Fig. 6(b) also shows that the tip temperatures vary less with the A/F ratio in comparison with the air load of 1.0. This implies that the flame position varies less due to a reduced flow velocity in comparison with the case for the air load of 1.0. When the air load is further decreased to 0.6, as shown in Fig. 6(c), it is likely that the flame moves further upstream into the burner. It is expected in this case that the flame position varies more sensitively with the change in the A/F ratio. The smallest A/F ratio pulls the flame the most upstream, farthest from the cone tip face, leading to the lowest tip temperatures. With increasing A/F ratio, the tip temperatures are increased as the flame moves downstream, but it still stays near the exit of the burner due to a reduced flow velocity, judging from the fact that the temperature is not decreased even for the largest A/F ratio above 40. Fig. 6(c) also shows that the location with the highest temperature is changed from CH25 to CH27. Such change may arise from the fact that the reduced swirling force by a reduced air flow rate relocates the flame position in a circumferential

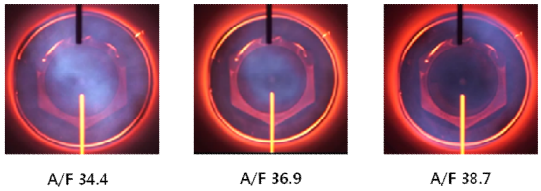


Fig. 5. The flame images for various A/F ratios (Load 1.0, 370°C).

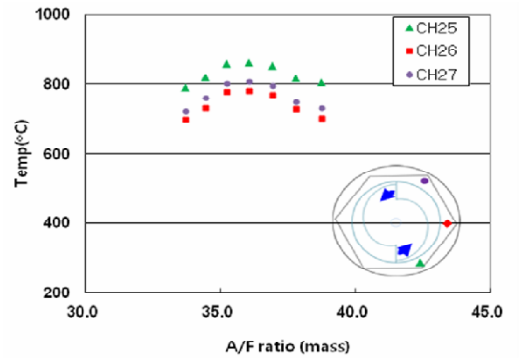


(a)

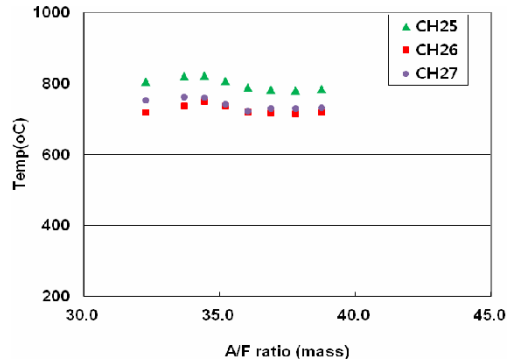


(b)

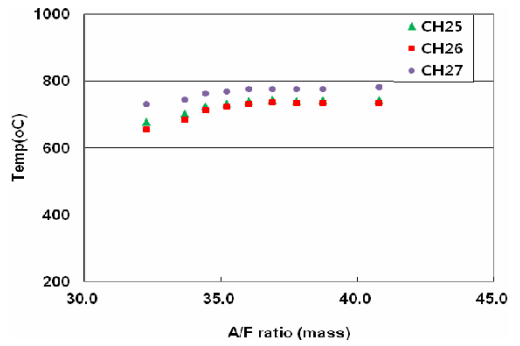


(c)

Fig. 6. Temperature distributions on the burner tip face for various A/F ratios with air loads of 1, 0.8, 0.6 in (a)-(c), respectively.

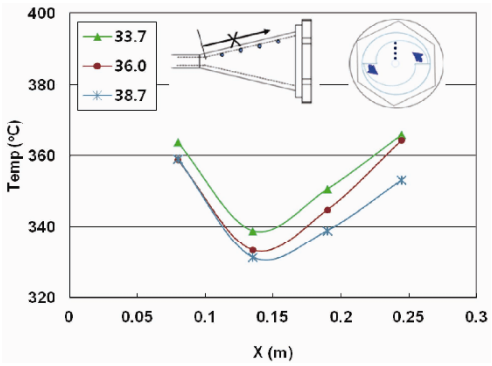


(a)

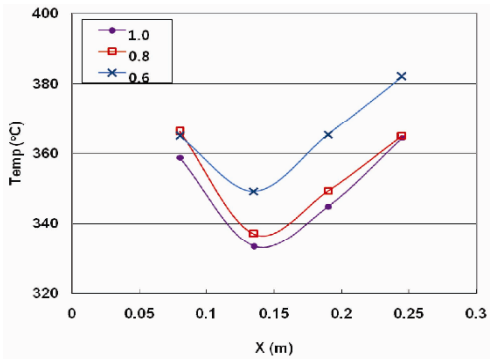


(b)

Fig. 7. The dependence of temperature distributions along the interior surface of the burner on (a) A/F ratio; (b) air load at A/F = 36.0.

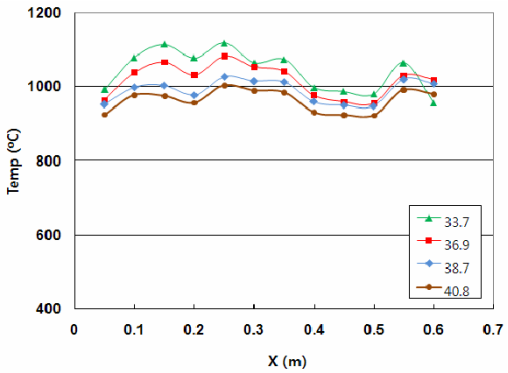


(a)

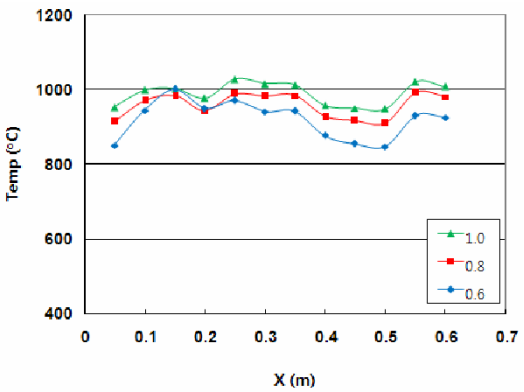


(b)

Fig. 8. The dependence of temperature distributions along the combustor liner on: (a) the A/F ratio (air load = 1.0); (b) the air load (A/F = 38.7).

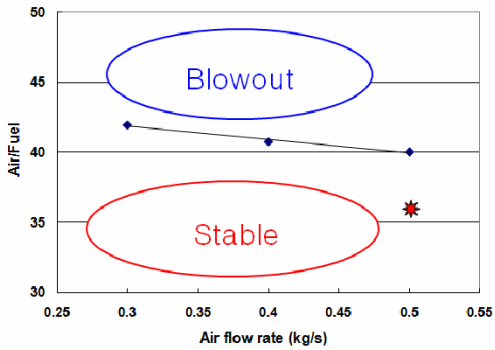


Fig. 9. Overall stability map of the EV burner.

direction.

Fig. 7 shows the inner temperature distributions along the interior surface of the burner for various A/F ratios as shown in Fig. 7(a), and for various air loads as shown in Fig. 7(b). Fig. 7(a) shows that the inner wall temperature of the cone is increased with a decrease in A/F ratio as the adiabatic flame temperature is increased. Note that the temperature distribution along the inner surface is not monotonic, i.e., it has a V-shape distribution, having a local minimum temperature at x ~ 0.14 m. Such local temperature drop in the middle of the cone results from cooling by the cold fuel injected through the side manifold along the air slot. Fig. 7(b) shows that the inner wall temperature of the cone is increased with a decrease in the air load. While the temperature distributions are similar for the air load of 0.8 and 1, the temperature for the smallest load of 0.6 is increased remarkably, especially from the middle to the exit of the cone. Such a noticeable increase in temperature distributions for the air load of 0.6 is regarded as another evidence that the flame is shifted more upstream inside the burner in comparison with the air loads of 0.8, 1.0.

Fig. 8 shows the temperature distributions along the combustor liner for various A/F ratios and air loads at an inlet air temperature of 370°C. In Fig. 8(a), the liner temperature is increased with a decrease in A/F ratio, i.e., an increase in the adiabatic flame temperature. The liner temperature is increased until it reaches a local maximum of, for instance, about 1100°C in case of A/F = 33.7, at about x = 0.25 m and then is decreased with increasing axial distance. It is likely that such a local maximum point represents where the flame hits the liner wall. In Fig. 8(b), the overall liner temperature is decreased with decreasing air load as a reduced flame size has a smaller heating effect on the liner wall.

### *3.3 Stability*

Fig. 9 shows the overall stability map, the extinction limit, of the EV burner at an inlet air temperature of 370°C. The

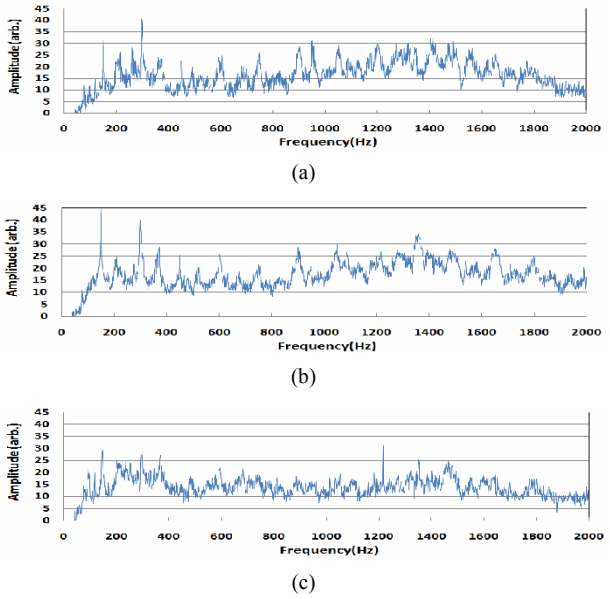


Fig. 10. Combustion noise characteristics with an air load of 1.0: (a) A/F 33.7; (b) A/F 36.0; (c) A/F 38.7.

extinction limit was obtained by reducing the fuel flow rate with a given air flow rate until the flame became unstable, leading to blowout. The maximum A/F ratio at which a stable flame is observed ranges from about 40 to 42, decreasing with an increase in the air flow rate. Such a reduced stable region with increasing the air flow rate arises because the higher air flow rate pushes the flame downstream, increasing the vulnerability to blowout. What is worth noting here is that increasing air flow rate can have two opposite effects in terms of stability: One is to enhance the stability by increasing the recirculation strength which acts as a means of flame anchoring. The other is to degrade the stability by reducing the flow residence time, which requires a higher reaction rate, i.e., a smaller A/F ratio, to sustain a stable combustion. Which one plays a more dominant role depends on the flow characteristics in the combustor. In this study, the latter one is considered to be a more dominant factor that affects the stability.

### *3.4 Combustion noise*

Fig. 10 shows frequency characteristics of combustion noise measured at the combustor exit for various A/F ratios. The dominant peaks appear at lower frequencies of about 150 and 300 Hz. These peak frequencies are considered to be the resonance frequencies for the longitudinal mode of the combustor, which is approximately evaluated by a simple formulation for the longitudinal resonance frequencies as follows.

$$f_n = \frac{nc}{2l} \quad (n = 1, 2, 3, ...), \tag{1}$$

where the boundary conditions for both ends of the combustor are approximated to be acoustically closed (v' = 0). Using a combustor length $l$ of 4.6 m and an averaged gas temperature of 1000°C measured in the middle of the combustor yields the frequencies associated with the first four modes (n = 1,2,3,4), which are about 75, 150, 225, 300 Hz, respectively, with corresponding mode shapes being depicted in Fig. 11. Fig. 12 represents how the peak amplitude changes with A/F ratio, showing that the peak amplitude has its maximum at the A/F ratio of 36, at which the flame is considered to move in and out of the burner exit, leading to augmentation of combustion noise. Either decreasing or increasing A/F ratio from 36 alleviates the noise level as the flame stays in a more stable position either inside or outside the burner. Note also that the peak frequencies can be divided into low (~150 Hz) and high (> 1 kHz). The low frequency noises are known as dominant sources that drive instabilities in a silo-type combustor of GT11N [13], as depicted in Fig. 12 showing that the low frequency noises dominate the high frequency noises in terms of peak amplitude. The high frequency noises are regarded as being associated with radial and/or tangential modes inside the combustor, which would rather appear as broadband noises than distinct peaks.

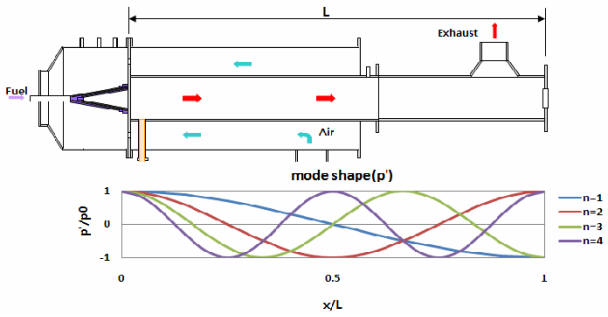


Fig. 11. Longitudinal mode shapes of the combustor.

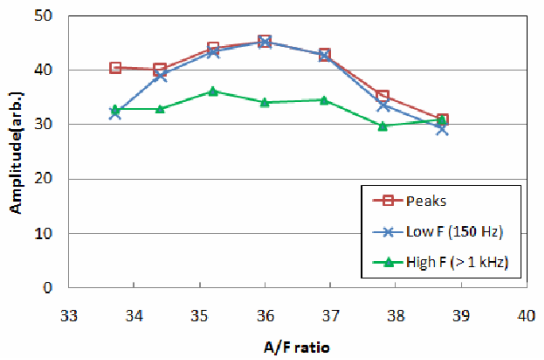


Fig. 12. The dependence of peak pressure amplitudes on A/F ratio.

### *3.5 Pressure loss*

Fig. 13 shows how much pressure loss occurs across the burner for cold flow (without combustion) and for reaction flow (with combustion at A/F 38.7). For cold flow, the pressure loss is increased with the square of air flow rate. This is caused by the flow resistance introduced into the airstream across the air slot of the burner [1].

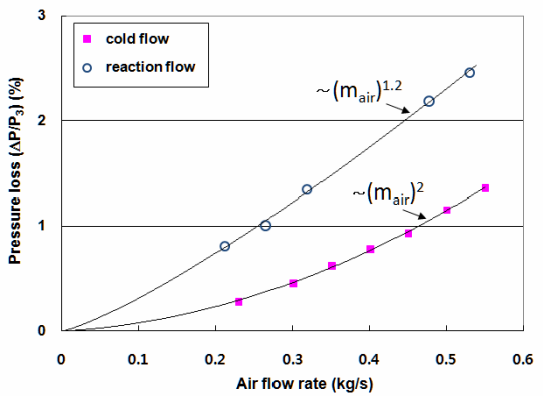


Fig. 13. The dependence of pressure loss of the burner upon the air flow rate.

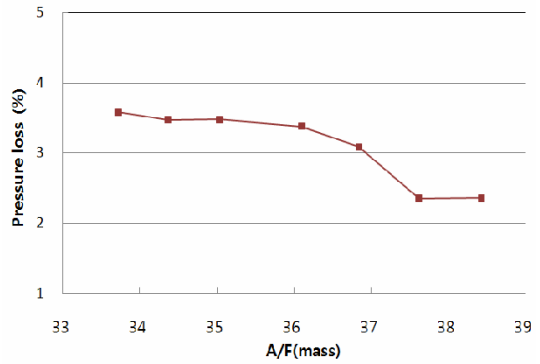


Fig. 14. The dependence of pressure loss of the burner upon the A/F ratio.

$$\frac{\Delta P}{P_3} \sim \left( \frac{\dot{m}_3 T_3^{0.5}}{P_3} \right)^2 . \quad (2)$$

The subscript "3" denotes the combustor inlet condition. The pressure loss in case of reaction flow is larger than that of cold flow, which results from an additional pressure loss due to an increase in momentum of hot product gases during combustion [14]. The rate of increase of the pressure loss in case of reaction flow, however, is not as large as that of cold flow. This arises because an increase in air flow rate moves the flame more downstream, which diminishes flow resistance against the flame.

Fig. 14 shows pressure loss across the burner upon A/F ratio during combustion. The pressure loss is kept almost invariant for lower A/F ratios, and then decreases noticeably near the A/F ratio of 37 as the flame moves downstream out of the burner, leading to a noticeable reduction of flow resistance against the flame. The pressure loss is one of the important factors that affect emissions and power as it affects the amount of air introduced into the combustor. For instance, a higher pressure loss allows less amount of air into the combustor, which results in a higher flame temperature, leading to higher NOx emissions, and less power generation due to more bypass air going into the secondary cooling. Fig. 14 also implies in the context of manufacturing that the burners should be manufactured as similar as possible, especially for the air slots, because inconsistent pressure losses due to the discrepancy in the air slots among burners yields non-uniform distribution of air introduced into the burners, which induces local hot spots that increase thermal NOx. Also, the pressure loss curve in Fig. 14 provides useful information for assessing the air mass distributions among groups of burners with different A/F ratios for GT11N. For instance, if two groups of burners in the silo type combustor have different A/F ratios, therefore different pressure losses, by supplying different amounts of fuel during load up processes, then the air flow is redistributed such that more air goes into the group with a lower pressure loss until the pressure losses are balanced for two groups.

## 4. Conclusions

Combustion characteristics of a swirl-stabilized premixed burner were investigated experimentally. NOx emissions are decreased with increasing air/fuel ratio due to a reduced adiabatic flame temperature, or with decreasing air load (for air load not less than 0.8). For air load of 0.6, NOx emissions are rather increased for a higher air-fuel ratio, which results from degraded mixing quality due to a shorter mixing distance to the flame. CO emissions are decreased with increasing air/fuel ratio because more oxygen is available for CO oxidation. Therefore, NOx and CO emissions are positively correlated for each air load. Flame extinction limit is reduced with increasing air flow rate as the flow residence time is reduced. Combustion noise has its peak amplitude at 150 or 300 Hz with broadband noise around 1 kHz. The peak frequencies are considered to be the resonance frequencies of the liner, while the broadband noise is produced by the multi-dimensional modes inside the burner. The noise level at the peak frequency is maximized when the flame is considered to move in and out of the burner exit. Pressure loss is about 3% of the inlet pressure, decreasing with an increase in the A/F ratio as the flame moves downstream out of the burner.

Future work will include design modifications of the burner to enhance the combustion performances such as NOx emissions.

## Acknowledgment

This work was supported by the Power Generation & Electricity Delivery of the Korea Institute of Energy Technology Evaluation and Planning (KETEP) grant funded by the Korea government Ministry of Trade, Industry and Energy, and also supported by KIMM's research funds for gas turbine development.

## References

[1] A. H. Lefebvre, *Gas turbine combustion,* 2nd ed., Taylor and

Francis, Ann Arbor, MI USA (1998).
[2] N. D. Joshi, H. C. Mongia, G. Leonard, J. W. Stegmaier and E. C. Vickers, Dry low emissions combustors development, *ASME Turbo Expo* (1998) 1998-GT-0310.
[3] K. Döbbeling, J. Hellat and H. Koch, 25 years of BBC/ABB/Alstom lean premix combustion technologies, *ASME Turbo Expo* (2005) GT2005-68269.
[4] H. Streb, B. Prade, T. Hahner and S. Hoffmann, Advanced burner development for the VX4.3A gas turbines, *ASME Turbo Expo* (2001) 2001-GT-0077.
[5] B. C. Schlein, D. A. Anderson, M. Beukenberg, K. D. Mohr, H. L. Leiner and W. Traptau, Development history and field experiences of the first FT8 gas turbine with dry low NOx combustion system, *ASME Turbo Expo* (1999) 1999-GT-241.
[6] C. J. Etheridge, Mars SoLoNOx lean premixed combustion technology in production, *ASME Turbo Expo* (1994) 1994-GT-255.
[7] F. Güthe, J. Hellat and P. Flohr, The reheat concept: the proven pathway to ultralow emissions and high efficiency and flexibility, *J. Eng. Gas Turbines Power*, 131 (2) (2009) 021503-1-7.
[8] C. O. Paschereit, B. Schuermans and D. Buchey, Combustion process optimization using evolutionary algorithm, *ASME Turbo Expo* (2003) GT2003-38393.
[9] M. Zajadatz, R. Lachner, S. Bernero, C. Motz and P. Flohr, Development and design of Alstom's staged fuel gas injection EV burner for NOx reduction, *ASME Turbo Expo* (2007) GT2007-27730.
[10] S. Kokanović, G. Guidati, S. Torchalla and B. Schuermans, Active combustion control system for reduction of NOx and pulsation levels in gas turbines, *ASME Turbo Expo* (2006) GT2006-90895.
[11] D. Fritsche, M. Füri and K. Boulouchos, An experimental investigation of thermoacoustic instabilities in a premixed swirl-stabilized flame, *Combust. Flame*, 151 (2007) 29-36.
[12] T. Sattelmayer, M. P. Felchlin, J. Haumann, J. Hellat and D. Styner, Second generation low-emission combustors for ABB gas turbines: burner development and tests at atmospheric pressure, *ASME Turbo Expo* (1990) 90-GT-162.
[13] S. B. Seo, D. H. Ahn, D. J. Cha and J. H. Park, Analysis of combustion oscillation and suppression in a silo type gas turbine combustor, *Korean J. Air-cond. Refrig. Eng.*, 21 (2) (2009) 126-130.
[14] H. I. H. Saravanamuttoo, G. F. C. Rogers, H. Cohen and P. V. Straznicky, *Gas turbine theory*, 6th Ed., Pearson Education Ltd., England (2009).

**Ju Hyeong Cho** received his B.S. and M.S. in Aerospace Engineering from Korea Advanced Institute of Science and Technology (KAIST) in Daejeon, Korea, in 1994 and 1996, respectively. His Ph.D. is from Georgia Institute of Technology in USA in 2006. Dr. Cho is currently a principal researcher at Korea Institute of Machinery and Materials (KIMM) and an associate professor at the University of Science and Technology in Daejeon, Korea. His research interests are in the area of design and analysis of gas turbine combustion system with his specialty in combustion instabilities.

**Han Seok Kim** received his B.S. in Mechanical Engineering from Hanyang University, Seoul, Korea in 1984, and his M.S. and Ph.D. in Mechanical Engineering from Korea Advanced Institute of Science and Technology (KAIST), Korea in 1988 and 2002, respectively. Dr. Kim is currently a principal researcher and a head of Department of Eco-Machinery System at Korea Institute of Machinery and Materials (KIMM). His research interests are in the area of development of low-emissions gas turbine combustion system and its applications to industrial power plants.

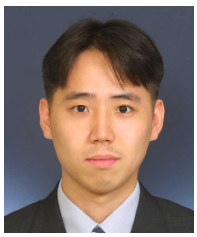

**Min Kuk Kim** received his B.S. from Yonsei University in 2003 and Ph.D. in Mechanical Engineering from Seoul National University, Korea, in 2010. Dr. Kim is currently a senior researcher at Korea Institute of Machinery and Materials (KIMM) in Daejeon, Korea. His research interests are in the area of design of gas turbine combustor, emission control, laser diagnostics, and electric-field assisted combustion system.

**Jeong Jae Hwang** received his B.S., M.S., and Ph.D. in Mechanical and Aerospace Engineering from Seoul National University, Korea, in 2007, 2009, and 2014. He is currently a senior researcher at Korea Institute of Machinery and Materials (KIMM) in Daejeon, Korea. His research interests are in the area of turbulent flames, combustion instabilities, and laser diagnostics.

**Sang Min Lee** received the B.S., M.S. and Ph.D. in Mechanical Engineering from Seoul National University in 1997, 1999, and 2003. Dr. Lee is currently a principal researcher at Korea Institute of Machinery & Materials (KIMM). His research interests are in the area of pollution control in combustion for industrial and agricultural applications.